https://doi.org/10.1016/j.apor.2018.08.005

On a submerged wave energy converter with snap-through power take-off

Lixian Wang[a,b,c,*], Hui Tang[c], Yanghua Wu[d]

[a] *Key Laboratory of High Performance Ship Technology (Wuhan University of Technology), Ministry of Education, China*
[b] *Departments of Naval Architecture, Ocean and Structural Engineering, School of Transportation, Wuhan University of Technology, China*
[c] *Department of Mechanical Engineering, The Hong Kong Polytechnic University, Kowloon, HKSAR, China*
[d] *School of Mechanical & Aerospace Engineering, Nanyang Technological University, Singapore 639798, Singapore*

Abstract

This paper investigates the performance of a bistable snap-through power take-off (PTO) operating inside a submerged wave energy converter (WEC). The equation of motion of the surging WEC is derived in the time domain using the Euler-Lagrange equations. The dynamic response of the WEC in regular waves is studied first. It is found that the wave amplitude has a significant impact on the energy conversion efficiency with the proposed energy extraction mechanism. With larger waves impacting on the WEC, the conversion efficiency of the present nonlinear PTO increases significantly. Three response regimes, i.e. local oscillation, aperiodic snap-through, and periodic snap-through, of the nonlinear PTO system are observed with various wave amplitudes. This nonlinear feature is quite different from the linear PTO mechanism that is independent of the wave amplitude. Further, the dynamic response of the nonlinear WEC subjected to irregular wave sea conditions is investigated. Parametric studies have been carried out to determine the optimum operating conditions of the bistable device in order to maximize the wave energy extraction. The utilization of the snap-through PTO can enhance the efficiency of the WEC over its

*Corresponding author Tel/Fax: +86 027 8655 1193
Email address: lixianwang@whut.edu.cn (Lixian Wang)

linear counterpart in irregular waves.

Keywords: `Nonlinear wave energy converter, Submerged cylinder, Snap-through PTO, Efficiency, Two-body system`

1. Introduction

Renewable energy is energy that comes from resources that are replenished continuously such as the sun, wind, ocean current and wave. These sources of energy have been explored globally as conventional sources of energy such as fossil fuel are limited and will be depleted in the foreseeable future. Furthermore, conventional sources of energy create pollution and carbon dioxide emission, posing a severe threat to the environment. Hence, it is vital to find a reliable and clean substitution for sustainable development. Compared with other renewable energy such as wind and solar energy, wave energy is superior in terms of energy density and stability [1, 2].

To extract wave energy, various technologies have been proposed since the 1970s, which have been well reviewed in Refs. [1–3], just naming a few. Based on the working principle, wave energy converters can be categorized as oscillating water column, overtopping devices, and oscillating body systems. Most of the oscillating water column wave energy converters (WECs) are located nearshore while the oscillating body systems are often deployed in deep water (>40 m), where wave energy is more intensive. Among the oscillating-body based WECs, the oscillating body can be either floating (e.g. [4–7]) or submerged (e.g. [8–14]). Compared with floating WECs, submerged WECs are superior in terms of survivability during sea storms when they are located offshore in deep water [15]. Submerged WECs such as the Bristol Cylinder device invented by Evans et al. [9] have been studied extensively [8, 10, 14]. Advantages of the Bristol Cylinder WEC include shedding excessive power levels, reducing excessive wave loads, and avoiding "end stop" problems. Recently, Evans & Porter [11] and Crowley et al. [12, 13] further enhanced the efficiency of the submerged WEC technologies.

Generally, an efficient wave energy extraction device is designed by being resonant at the incident wave frequency. However, there are two major difficulties for this kind of resonant WECs: one is that the response efficiency curve is narrow banded of wave periods if it is resonant at a certain frequency; the other is that resonant WECs are required to be of large size for a typical Northern Atlantic wave period (10 s). Therefore, the irregularity in the ocean waves will pose a serious problem for such WECs. To overcome these challenges, many studies were carried out by using control strategies such as the linear/nonlinear passive control [16], latching control [17–19], declutching control [20], and reactive control [21], etc. Various control techniques dedicated to increasing power production of WECs have been summarized in Ref. [22]. However, most control strategies (e.g. latching and declutching control) require that the wave information is known as a prerequisite in order to predict the wave forces acting on the WECs. The performance of these control techniques may be significantly diminished if the prediction deviation of wave information of real sea state is considered [23]. Besides, additional sensors, activators and processing elements are needed to implement these control strategies, thus leading to high installation costs and maintenance difficulties. Apart from control strategies, multi-resonant devices [11, 12] or nonlinear snap-through power take-offs (PTOs) [5, 24] were also used to enhance WEC efficiency. Evans & Porter [11] introduced a multi-resonant WEC consisting of a submerged buoyant circular cylinder tethered to the sea bed by inextensible mooring lines. An internal mass-spring-damper PTO is located within the cylinder. In this way, a two-body wave energy converter is created. This allows the use of the internal mass to further improve the performance of the WEC [25]. The idea behind this concept is to tune devices to be resonant at a broader range of incident wave periods in realistic sea state. Inspired by this, Crowley et al. [12] introduced a novel internal PTO device comprising multiple pendulums within the submerged cylinder. Apart from multi-resonant PTOs, Zhang and his co-workers [4, 5] initiated the use of the nonlinear snap-through PTO to increase the power extraction of a heaving WECs. The snap-through mechanism is made up by

two oblique linear springs and a linear damper connected to a mass. Details of this bistable mechanism are reported in [26]. It was found that the nonlinear PTO system outperforms its linear PTO counterpart in waves of relatively low frequencies. Similar conclusions were made in Ref. [24] by using other types of bistable PTOs. In these bistable PTO based WECs, the floating buoy itself is used as the mass experiencing snap-through.

Inspired by the above nonlinear PTO studies, in this paper, we proposed a submerged cylinder WEC containing an internal mass-spring-damper snap-through PTO, as shown in Fig. 1. To investigate the performance of this two-body system WEC, the equations of motion are derived in the time domain using the Euler-Lagrange equations. Instead of the frequency-domain method, a time-domain numerical method using fourth-order predictor-corrector Adams-Bashforth-Moulton method [27] is adopted to solve the system of ordinary differential equations. The performance of this WEC subjected to either regular or irregular waves is studied.

2. WEC with snap-through PTO

As shown in Fig. 1, the proposed WEC consists of a submerged circular cylinder, a mooring line and an internal PTO mechanism. The same as the submerged WECs in the work of Evans & Porter [11] and Crowley et al. [12], this device is assumed to span a narrow wave tank. So the problem can be treated as two dimensional and the submerged cylinder is of unit length in the third direction. The cylinder is selected such that its buoyancy is larger than its weight. As such, the mooring line connecting the cylinder center and a fixed pivot is taut and the cylinder is restrained to pitch around this pivot. Located inside the cylinder is a PTO that comprises of a mass-spring-damper system. Different from the simple mass-spring-damper system, the present PTO consists of two oblique linear springs connecting to an internal mass. This arrangement yields a nonlinear restoring force acting on the mass. Due to this nonlinear force, two stable equilibrium positions exist for the internal mass [26]. It will

thus oscillate around one of the two stable equilibrium positions if the motion is small, and oscillate between the two stable equilibrium positions if the motion is large, indicating a snap-through motion.

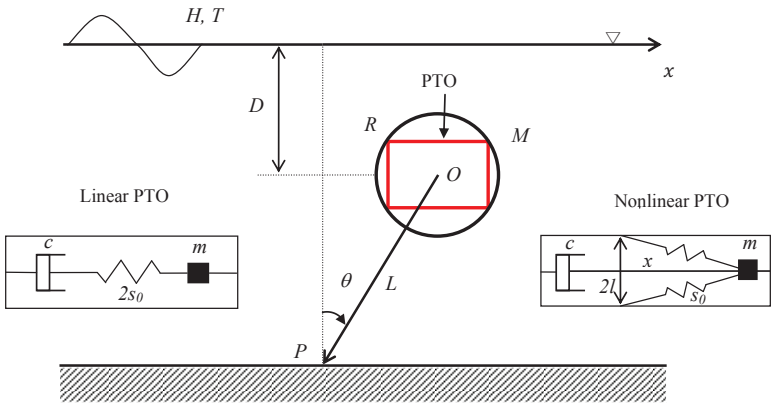

Figure 1: Submerged cylinder WEC with the nonlinear PTO

3. Mathematical formulations

In order to investigate the performance of the proposed WEC, the dynamic response of this WEC subjected to incident waves is analyzed. The present WEC is a two degree-of-freedom dynamic system: the pitch motion of the submerged cylinder and the horizontal surge motion of the internal mass relative to the cylinder. Assume that the pitch angle of the cylinder is small, the vertical force acting along the mooring line balances the difference between the buoyancy and the gravity of this WEC. In this study, this difference is assumed in the same order with the buoyancy acting on the cylinder (see Section 4.1). With the small-motion assumption, the wave forces are not comparable with the buoyancy. Thus, the mooring line keeps taut and its length does not vary during the motion of the cylinder. The heave of the cylinder is of second-order and thus can be neglected in the present analysis. To deal with these coupled motions, the equations of motion are readily derived from the Euler-Lagrange equations. θ and x are selected as two generalized coordinates, representing pitch of the submerged cylinder and relative surge of the internal mass, respectively. When

the aforementioned snap-through based PTO is incorporated into the submerged cylinder, as depicted in Fig. 1, the potential energy $V_e(x)$ stored in the new system is

$$V_e(x) = s_0 \left(\sqrt{x^2 + l^2} - l_0 \right)^2 \tag{1}$$

and the kinetic energy $T_e(\theta, x)$ carried by this system is

$$T_e(\theta, x) = \frac{1}{2} m(\dot{x} + L\dot{\theta})^2 + \frac{1}{2} M L^2 \dot{\theta}^2 \tag{2}$$

where s_0 is the stiffness constant of the springs, l_0 their original length, l the half distance between the two ends of springs that are fixed on the cylinder, m the internal mass, L length of the mooring line, M the mass of the submerged cylinder per unit length. $\dot{x}$ and $\dot{\theta}$ denote the horizontal velocity of the internal mass and the angular velocity of the submerged cylinder, respectively. In the above two equations, Eq. 1 represents the elastic potential energy stored in the two oblique springs of the internal PTO. Note that since the heave of the cylinder is ignored in this study, the gravitational potential energy is omitted. The second equation, i.e. Eq. 2, denotes the kinetic energy stored in both the internal mass (m) and the submerged cylinder (M). Similar to [11], in the present study the cylinder is forced into horizontal surge motion in the framework of small-amplitude linearized theory, thus the rotational kinetic energy is not taken into account in Eq. 2. By applying the Euler-Lagrange equations, the equations of motion for this system are

$$(m + M) L^2 \ddot{\theta} + mL\ddot{x} + (M_w - M - m) gL\theta = F_{wave} L \tag{3}$$

and

$$mL\ddot{\theta} + m\ddot{x} + c\dot{x} + 2s_0 \left(1 - \frac{l_0}{\sqrt{x^2 + l^2}} \right) x = 0 \tag{4}$$

where $\ddot{x}$ and $\ddot{\theta}$ denote the horizontal acceleration of the internal mass and the angular acceleration of the submerged cylinder, respectively. The damping of the damper in the internal PTO is represented by c. The last term on the left hand side of Eq. 3 describes the restoring force exerted by the mooring line, which is the horizontal component of the tension force in the mooring line. The

mooring tension force is estimated from the force balance involving the buoyancy $M_w g(\equiv \rho\pi R^2 g)$ and gravities of the submerged cylinder and the internal mass. F_{wave} on the right hand side of Eq. 3 represents the horizontal wave force acting on the submerged cylinder.

3.1. Wave energy converter equipped with snap-through PTO in regular waves

In order to determine the wave force F_{wave} due to normally incident regular waves in deep water, linear wave theories are applied. As such, the present problem is simplified as a linear superposition of a wave diffraction problem and a wave radiation problem. The total horizontal wave force can be obtained through

$$F_{wave} \equiv F_{ex} + F_{rad} \tag{5}$$

where F_{ex} and F_{rad} represent wave exciting force and wave radiation force, respectively. The wave exciting force F_{ex} can be calculated by using the Haskind's relationship [28]: its magnitude for a regular incident wave of amplitude A and frequency ω can be written as

$$|F_{ex}(\omega)| = A\sqrt{\frac{\rho g^2 B_{11}(\omega)}{\omega}} \tag{6}$$

where B_{11} denotes the wave damping of the submerged cylinder in the horizontal direction. Therefore, the wave exciting force can be expressed as

$$F_{ex}(t) = |F_{ex}|\cos(\omega t) \tag{7}$$

Since there is a nonlinear term appearing in Eq. 4, the wave radiation force cannot be calculated by assuming constant added mass and hydrodynamic damping. Instead, the free-surface memory effect has to be included. Therefore the resulting wave radiation force F_{rad} can be written as [29]

$$F_{rad}(t) = -A_{11}(\infty)L\ddot{\theta} - \int_{-\infty}^{t} K_{11}(t-\tau)L\dot{\theta}(\tau)d\tau \tag{8}$$

where $A_{11}(\infty)$ denotes the infinite-frequency limit of the frequency-dependent added-mass. The kernel in the convolution integral on the right hand side of

Eq. 8 is calculated by [30]

$$K_{11}(t) = \frac{2}{\pi}\int_0^\infty B_{11}(\omega)\cos(\omega t)d\omega \tag{9}$$

The kernel can be determined if the frequency-dependent damping coefficient B_{11} is known. We use the multipole expansion method [31] to calculate both the added-mass and damping coefficients of the submerged cylinder for wave frequencies $(0, \infty)$. At both frequency limits, i.e., $\omega \to 0$ and $\omega \to \infty$, $B_{11}(\omega)$ are essentially zero [32]. To calculate $A_{11}(\infty)$, the Kramers-Kronig relations [33] are used. Given the added-mass coefficient at a finite frequency ω, $A_{11}(\omega)$, and damping coefficients over a range of frequencies $(0, \infty)$, the infinite-frequency limit of the frequency-dependent added-mass $A_{11}(\infty)$ can be obtained. In addition, the free-surface memory effect shown in the convolution integral in Eq. 8 decays rapidly with time after a few tens of seconds [34]. Therefore, both the integration intervals in Eqs. 8 and 9 can be replaced by finite values. This method is adopted in the present simulations since it is able to accelerate the computation of integration without loss of accuracy.

After both the wave exciting force F_{ex} and wave radiation force F_{rad} are determined, the horizontal wave force F_{wave} acting on the submerged cylinder is sought by using Eq. 5. Substituting Eqs. 5, 7, and 8 into Eq. 3, the equations of motion (Eqs. 3 and 4) for the WEC system can be rewritten into matrix form

$$\begin{bmatrix} [m+M+A_{11}(\infty)]L^2 & mL \\ mL & m \end{bmatrix}\begin{bmatrix} \ddot{\theta} \\ \ddot{x} \end{bmatrix} + \begin{bmatrix} 0 & 0 \\ 0 & c \end{bmatrix}\begin{bmatrix} \dot{\theta} \\ \dot{x} \end{bmatrix} + \begin{bmatrix} (M_w - M - m)gL & 0 \\ 0 & 2s_0\left(1 - \frac{l_0}{\sqrt{x^2+l^2}}\right) \end{bmatrix}\begin{bmatrix} \theta \\ x \end{bmatrix} = \begin{bmatrix} F_{ex}(t)L - \int_{-\infty}^{t} K_{11}(t-\tau)L^2\dot{\theta}(\tau)d\tau \\ 0 \end{bmatrix} \tag{10}$$

With Eq. 10, the dynamic response of the WEC in regular waves can then be solved in the time domain. The fourth-order Adam-Bashforth-Moulton integration method is applied to solve the second-order ordinary differential Eq. 10. Once the time history of the internal mass velocity $(\dot{x})$ is obtained, the average

extracted power by the internal PTO over a time interval of length τ can be evaluated using

$$P_{avg} = \frac{1}{\tau}\int_0^\tau c\dot{x}^2 dt \tag{11}$$

After obtaining the average extracted power, the efficiency of the present WEC is calculated using

$$E = \frac{P_{avg}}{P_w} \tag{12}$$

where P_w is the power carried by the incident waves. For a regular incident wave of amplitude A and frequency ω in deep water, the wave power is computed by

$$P_w = \rho A^2 g^2 / 4\omega \tag{13}$$

Based on the above analysis, the efficiency of the present WEC in regular waves depends on 13 parameters, i.e., L, D, R, M, m, s_0, c, l_0, l, ω, A, ρ and g. Here D is submergence of the submerged cylinder. According to the Buckingham Pi theorem, 10 independent non-dimensional parameters can be identified to determine the power conversion efficiency

$$E = f(L', D', M', m', s_0', c', l_0', \gamma, kR, kA) \tag{14}$$

where $L' = L/R$, $D' = D/R$, $M' = M/\pi\rho R^2$, $m' = m/\pi\rho R^2$, $s_0' = s_0/\pi\rho g R$, $c' = c/\pi\rho\sqrt{gR^3}$, $l_0' = l_0/R$, and $\gamma = l/l_0$. The last two non-dimensional quantities, kR and kA, represent the non-dimensional incident wave frequency and steepness, respectively, where k is wave number. Although the total wave force F_w is not listed as an independent parameter, it will be non-dimensionalized as $F_w' = F_w/\pi\rho g R^2$ for convenience. The primes in Eq. 14 denote non-dimensional values of each quantity and, for the sake of simplification, they will be omitted hereafter.

3.2. Wave energy converter equipped with snap-through PTO in irregular waves

3.2.1. Wave spectrum

In this study, only one-directional normally incident irregular wave are considered and the water depth is assumed infinite. To describe the irregular waves,

a wave spectrum which shows the distribution of wave energy as a function of frequency is often used. In this study, the Pierson-Moskwitz wave spectrum for fully developed sea is chosen. The energy density for this wave spectrum is defined by [35]

$$S_{PM}(\omega) = \frac{0.3125}{2\pi} H_s^2 T_p \left(\frac{\omega T_p}{2\pi}\right)^{-5} exp\left[-\frac{5}{4}\left(\frac{\omega T_p}{2\pi}\right)^{-4}\right] \tag{15}$$

in which H_s and T_p denote the significant wave height and peak wave period, respectively. Assume that most of the energy in the above wave spectrum is distributed in the frequency range (ω_L, ω_H) and it is divided into a sequence of N elements such that

$$\Delta\omega = (\omega_H - \omega_L)/N, \hat{\omega}_i = (\omega_{i-1} + \omega_i)/2, \quad \frac{1}{2}A_i^2 = S(\hat{\omega}_i)\Delta\omega \tag{16}$$

in which A_i denotes the amplitude of the i-th wave component for frequency $\hat{\omega}_i$. In this study, it is assumed that all the wave components propagate towards the WEC in one-direction. Thus, the free surface elevation can be obtained by summing up all of the wave components without considering wave direction

$$\eta(t) = \sum_{i=1}^{N} A_i \cos\left(\hat{\omega}_i t + \epsilon_i\right) \tag{17}$$

where ϵ_i is the phase of the i-th wave component and is chosen randomly between 0 and 2π. To illustrate the random waves, the wave spectrum and associated wave elevation of a random wave with significant wave height $H_s = 4$ m and peak wave period $T_p = 10$ s are plotted in Figs. 2(a) and 2(b), respectively.

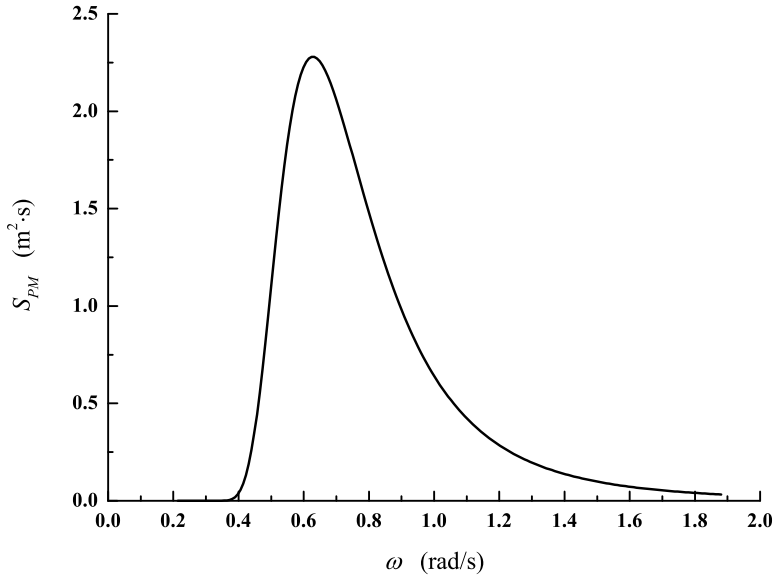

(a) wave spectrum

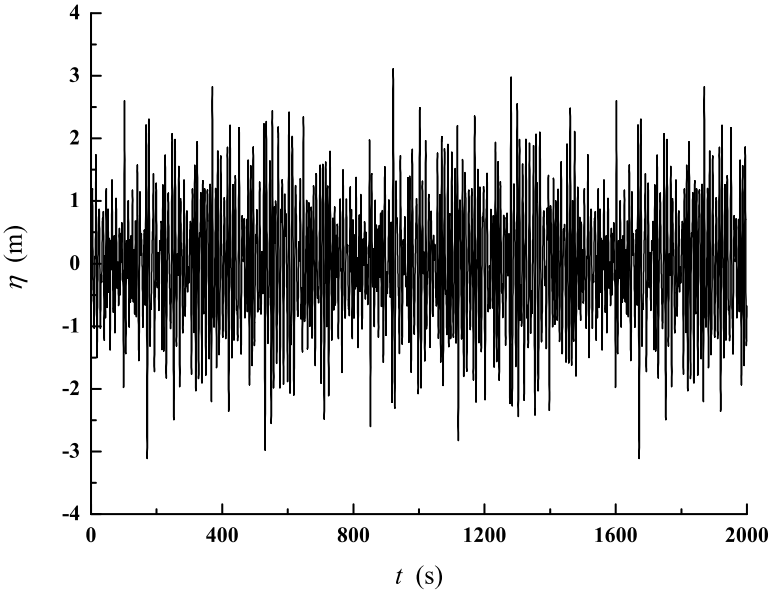

(b) wave elevation

Figure 2: A random wave with significant wave height $H_s = 4$ m and peak wave period $T_p = 10$ s

3.2.2. Equations of motion

Most formulations on the equations of motion of the above WEC in irregular waves are the same as those for regular waves. The only difference between the two scenarios is the calculation of the wave force. In irregular waves, the wave exciting force is written as

$$F_{ex}(t) = \sum_{i=1}^{N} \Gamma_{ex}(\hat{\omega}_i) A_i \cos\left(\hat{\omega}_i t + \varphi_i + \epsilon_i\right) \tag{18}$$

where $\Gamma_{ex}(\hat{\omega}_i)$ is the wave excitation force coefficient and φ_i is the phase response of the wave excitation force for the ith regular wave component. Using Eq. 6, the wave excitation coefficient is given by $\Gamma_{ex}(\hat{\omega}_i) = \sqrt{\rho g^2 B_{11}(\hat{\omega}_i)/\hat{\omega}_i}$.

In irregular waves, wave loads are functions of significant wave height H_s and peak wave period T_p. Therefore, the power conversion efficiency is a function of the following parameters:

$$E = f(L', D', M', m', s_0', c', l_0', \gamma, H_s', T_p') \tag{19}$$

Note that H_s and T_p in Eq. 19 are non-dimensionalized as $H_s' = H_s/R$ and $T_p' = T_p/\sqrt{R/g}$, respectively. The primes in Eq. 19 are also omitted hereafter for simplification, as done for Eq. 14.

When calculating the efficiency of WEC in irregular waves by Eq. 12, the power carried by irregular waves defined by the Pierson-Moskwitz wave spectrum is computed by

$$P_w = \frac{\rho g^2}{2} \int_0^\infty \omega^{-1} S_{PM}(\omega) d\omega \tag{20}$$

4. Results and discussions

4.1. Model validation

To validate the present modeling framework, the time-domain solution is validated by comparing its results with the frequency-domain based results for a simplified case, i.e., a tethered, submerged cylinder equipped a linear PTO inside. For this simplified case in regular waves, the last term on the left hand

side of Eq. 4 is simply replaced by $2s_0x$. The frequency-domain analysis is described in detail in the appendix. By adopting the WEC parameters of a coupled mass/spring/damper system in [11], $L = 3$, $m = 0.6$, $M = 0.15$, and $D = 1.25$ are used for the present WEC. Moreover, this WEC is tuned to achieve its maximum efficiency (i.e., 50% [8, 12]) at the wave frequency $k_0R = 0.7$. The tuned frequency is used to determine the spring stiffness and damping of the linear PTO mechanism with Eqs. A.13 and A.14, respectively. The simulation results including power extraction efficiency and the motion amplitudes are plotted in Figs. 3 and 4, respectively. It can be seen that the time-domain method produces the same results as using the frequency-domain method. In addition, observed from Fig. 4, the amplitudes of the cylinder and internal mass motions are found in the same order of the wave amplitude. This confirms the validity of the small-amplitude oscillation assumption, and hence the feasibility of applying the present time-domain method to the investigation of the WEC equipped with the nonlinear PTO mechanism.

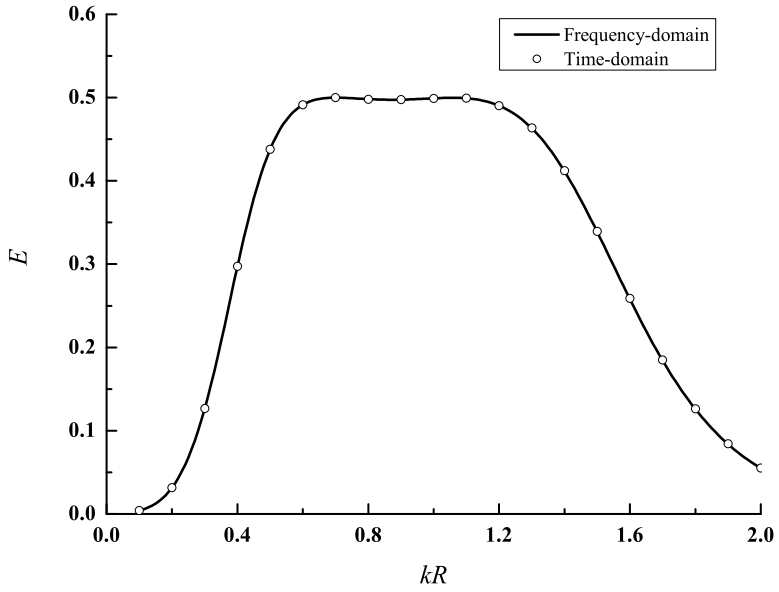

Figure 3: Comparison of efficiencies of the WEC between the present time-domain and frequency-domain methods for the linear PTO

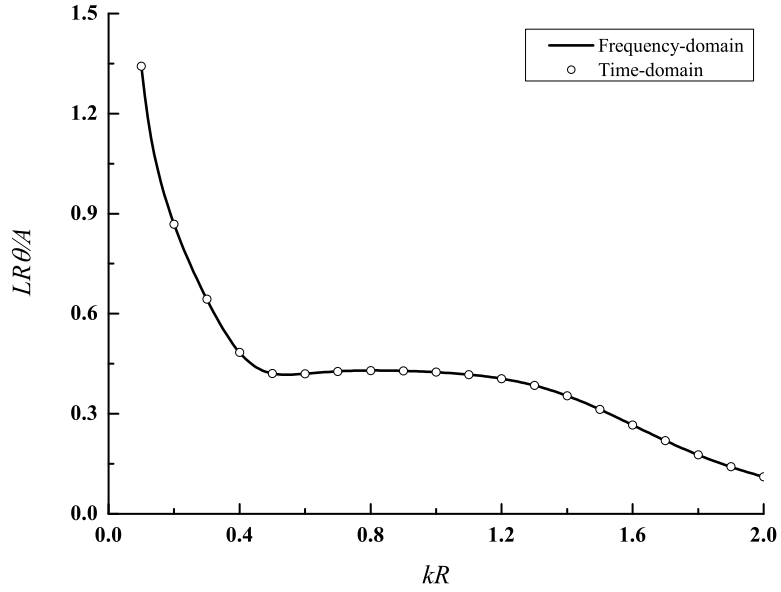

(a) pitch

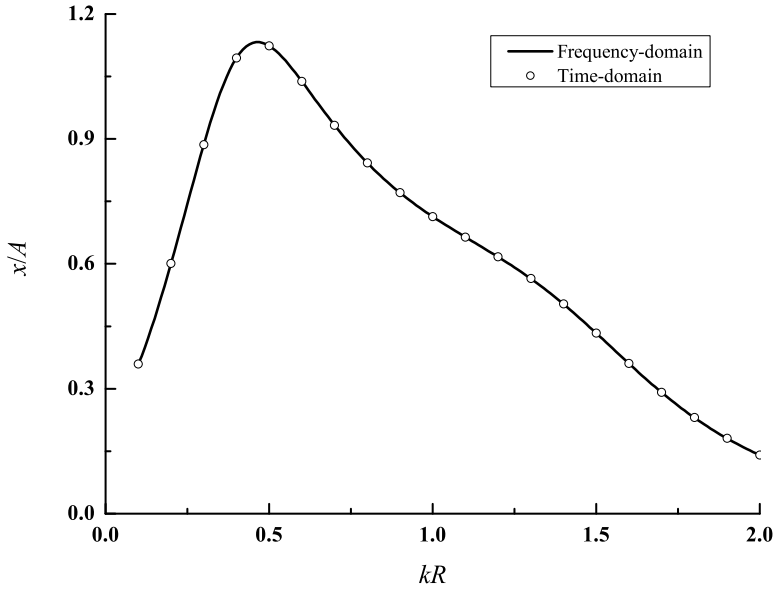

(b) surge

Figure 4: Comparison of motion responses of the WEC between the present time-domain and frequency-domain methods for the linear PTO

Furthermore, from the linear PTO analysis, a series of efficiency curves against tuned wave frequencies k_0R can be obtained. Figure 5 shows these efficiency curves with tuned wave frequencies ranging from 0.2 to 0.7. When the tuned frequency is set as $k_0R = 0.7$, the efficiency reaches about its theoretical maximum (50%) over a broad range of frequencies (from $kR = 0.6$ to 1.2). This is because the WEC is able to achieve multiple resonances with the tuned wave frequencies $k_0R = 0.7$ [11]. However, the wave frequency (kR) of the realistic sea situation is usually located far from the kR range of [0.6, 1.2]. For example, taking $T = 10$ s as a typical peak wave period in the northern Atlantic and $R = 5$ m as the radius of the submerged cylinder, the corresponding dimensionless peak wave frequency is $kR = 0.2$, much smaller than the tuned frequency $k_0R = 0.7$. Consequently, the efficiency of this WEC with the linear PTO is as low as 3.2% with the typical peak wave period $T = 10$ s. In order to improve the efficiency of the WEC, the nonlinear PTO mechanism shown in Fig. 1 instead of the linear PTO is proposed in this study.

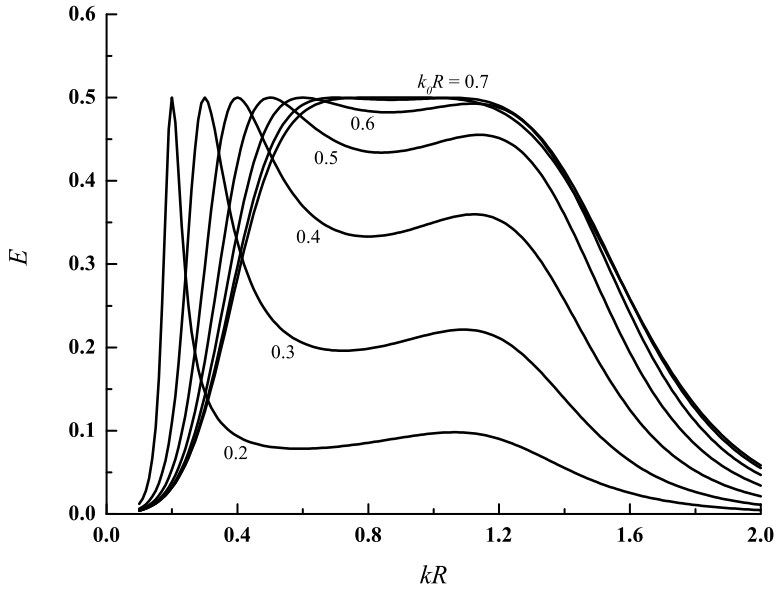

Figure 5: Efficiency varying with wave frequency for the linear PTO tuned to different wave frequencies

4.2. The nonlinear WEC in regular waves

As the first step, the power conversion efficiency of the nonlinear WEC in regular waves is studied. As revealed in Eq. 14, this efficiency is a function of the input wave parameters kA and kR. Note that kA shall be smaller than 0.01π to satisfy the small-amplitude wave assumption. After carrying out the time convergence study, the time step $dt = T/50$ is found appropriate and is therefore used in the ensuing simulations.

Before calculating the efficiency of the WEC using Eq. 12, we first need to determine the average power extracted using Eq. 11. As stated by [36], it is necessary to select a proper time interval τ in Eq. 11. This is because the average power extracted in the case of aperiodic snap-through (Figs. 8(b) and 9(c)) may not give a converged value. In this study, the simulation lasts for $200T$. For the calculation of the averaged power, the numerical results of the last $100T$ is used in order to avoid the initial transient effects. In Fig. 6, the average power extracted by the case of aperiodic snap-through is plotted against time interval τ. In this plot, the convergence bounds of $\pm 5\%$ (red horizontal lines) of the final value (at $\tau/T = 100$) are also shown. It is shown that the selected time interval $100T$ is sufficient to settle the averaged power inside the 5% bound. Therefore, this time interval is used in Eq. 11 to compute the average power extracted by the WEC in the following simulations.

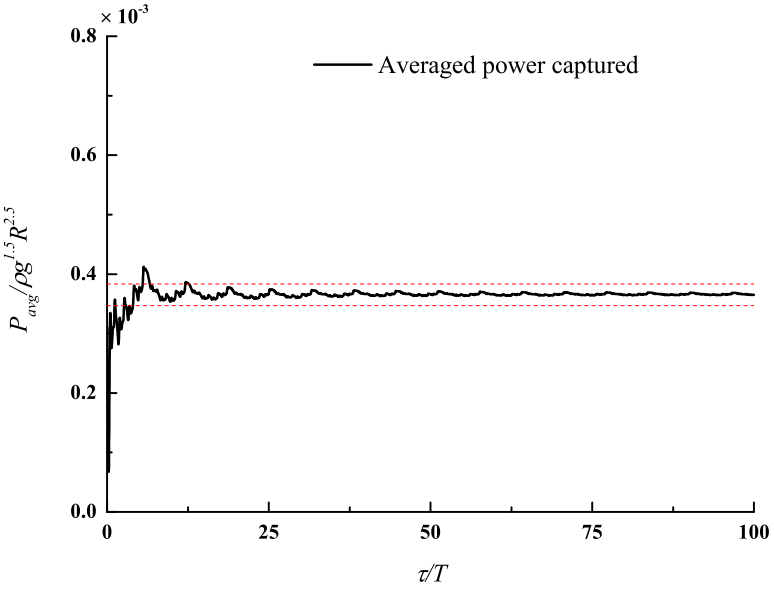

Figure 6: Convergence of average extracted power calculated with various lengths of time interval: regular waves of $kA/0.01\pi = 0.5$ and $kR = 0.2$

Before the studies on the effects of wave parameters, we first investigate effects of the nonlinear snap-through parameters l_0 and γ on the performance of the WEC. Three tuned wave frequencies have been considered including $k_0R =$ 0.2, 0.4, and 0.7, which are chosen based on the efficiency curves for the linear PTO shown in Fig. 3. The low tuned frequency $k_0R = 0.2$ is selected to represent the single-peak, narrow-banded efficiency curve, while the high tuned frequency $k_0R = 0.7$ is selected to represent a broad-banded efficiency curve. The amplitude and frequency of the regular wave are fixed at $kA/0.01\pi = 0.5$ and $kR = 0.4$, respectively. Both the snap-through PTO parameters γ and l_0 vary with an interval of 0.1.

The variations of efficiency with different nonlinear PTO parameters l_0 and γ are plotted in Fig. 7. It is seen that when l_0 is larger than 0.3, the efficiency variation with l_0 is within 5% for all the three tuned frequencies. This shows that the efficiency of the WEC is insensitive to the original length of the oblique springs when l_0 exceeds 0.3. When l_0 is less than 0.3, the effect of l_0 on the

efficiency differs with the tuned frequency. For example, the efficiency increases with the increase of l_0 with the medium tuned frequency $k_0R = 0.4$ while this is not true with the low and high tuned frequencies of $k_0R = 0.2$ and 0.7, respectively. Compared with l_0, the efficiency of the present WEC is found more sensitive to γ. With the low and medium tuned frequencies $k_0R = 0.2$ and 0.4, the efficiency generally decreases with the increase of γ ranging from 0.1 to 0.9, except that the efficiency shows fluctuations with γ when l_0 is as small as 0.1. While with the high tuned frequency $k_0R = 0.7$, the efficiency curve appears a peak within the considered range of γ. With $l_0 = 0.1$, the peak efficiency $E_{max} = 41\%$ occurs at $\gamma = 0.5$ while for other values of l_0, the efficiency peak shifts to $\gamma = 0.6$. From Fig. 7, efficiency of the present WEC is more sensitive to γ rather than l_0 when the WEC is subjected to regular waves.

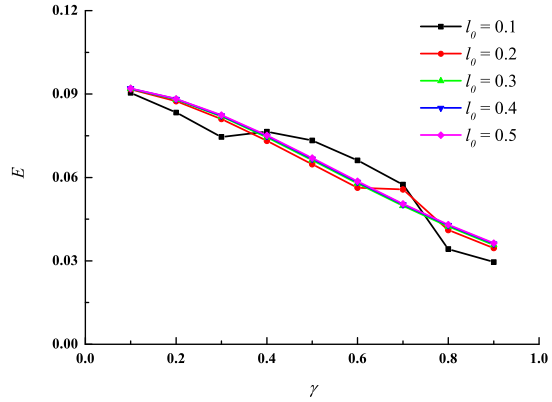

(a) $k_0R = 0.2$

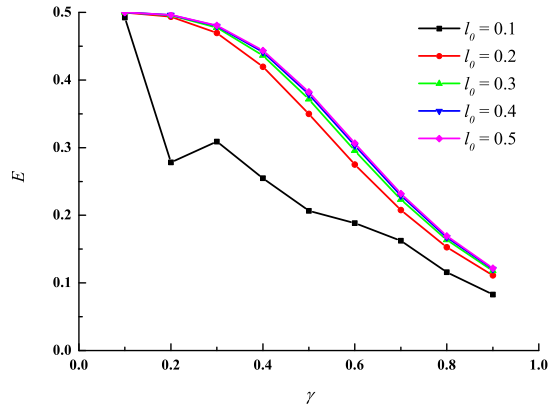

(b) $k_0R = 0.4$

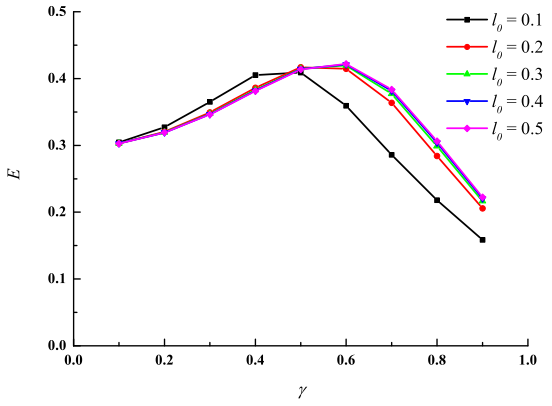

(c) $k_0R = 0.7$

Figure 7: Effects of the nonlinear PTO parameters l_0 and γ on the power extraction efficiency of the WEC in regular waves of $kR = 0.4$ and $kA/0.01\pi = 0.5$ with different tuned frequencies

4.2.1. Effect of wave amplitude kA

In this section, the effect of wave amplitude kA on the efficiency of the nonlinear snap-through WEC is studied. Except the wave parameters (kA and kR), the other parameters on the right hand side of Eq. 14 are set the same as those in the convergence test, i.e., $L = 3$, $m = 0.6$, $M = 0.15$, $D = 1.25$, $\gamma = 0.5$, $l_0 = 0.1$, $s_0 = 0.279$, and $c = 0.156$. The wave amplitude kA of regular waves varies from 0.1 to 0.9 of its maximum allowed value ($=0.01\pi$). Three different wave frequencies, i.e. $kR = 0.2$, 0.4, and 1.0, are considered. Figures 8 $\sim$ 10 present the time responses of the internal mass' relative surge displacement x, as well as the phase diagrams describing the relation between $\dot{x}$ and x. By increasing kA at the wave frequency $kR = 0.2$, three distinct response regimes are observed in Fig. 8. At small wave amplitude such as $kA/0.01\pi = 0.1$ (see Fig. 8(a)), the internal mass oscillates about one of its stable equilibrium positions that are depicted by two red dots.

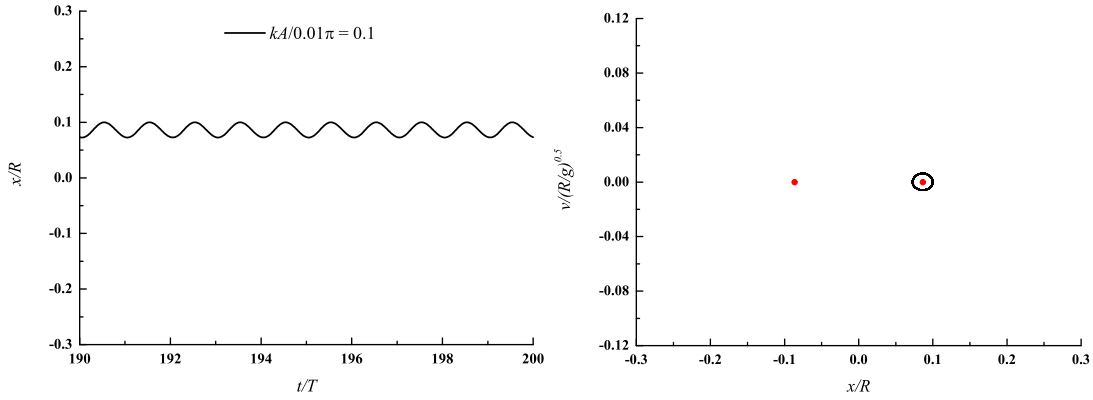

(a) $kA/0.01\pi = 0.1$

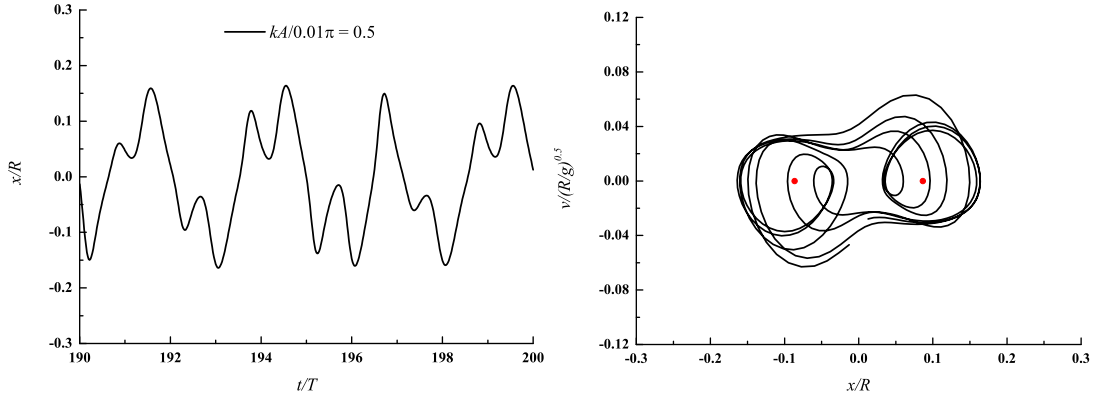

(b) $kA/0.01\pi = 0.5$

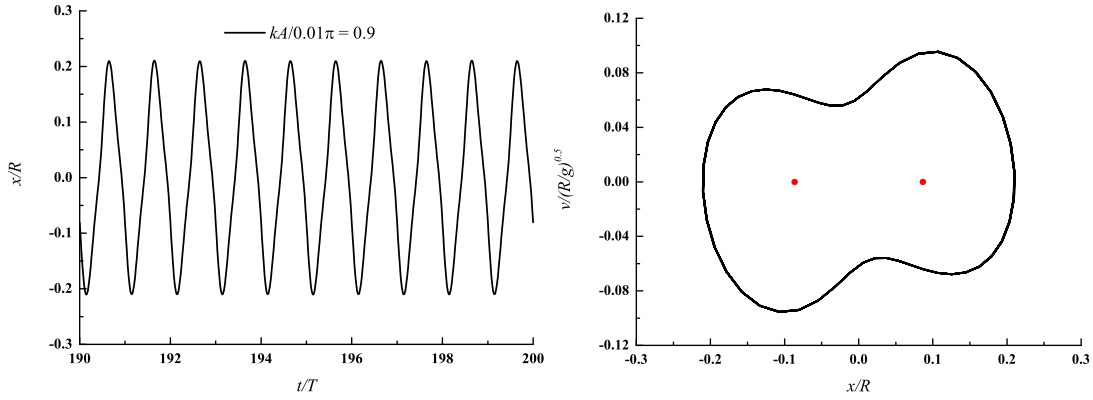

(c) $kA/0.01\pi = 0.9$

Figure 8: Time responses (left) and phase diagrams (right) of the internal mass to regular waves of frequency $kR = 0.2$

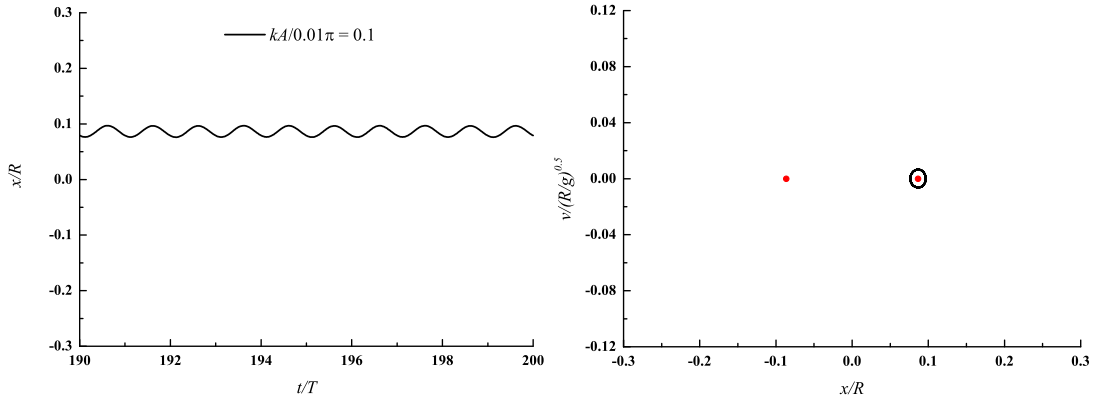

(a) $kA/0.01\pi = 0.1$

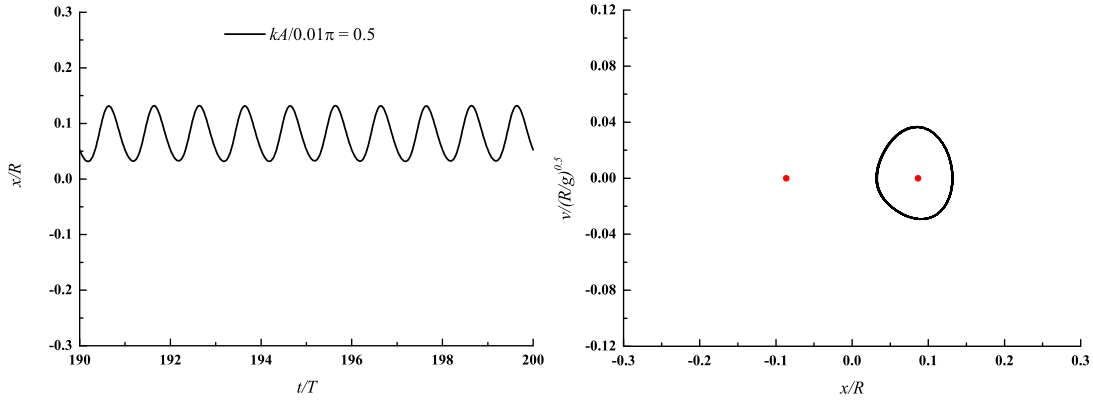

(b) $kA/0.01\pi = 0.5$

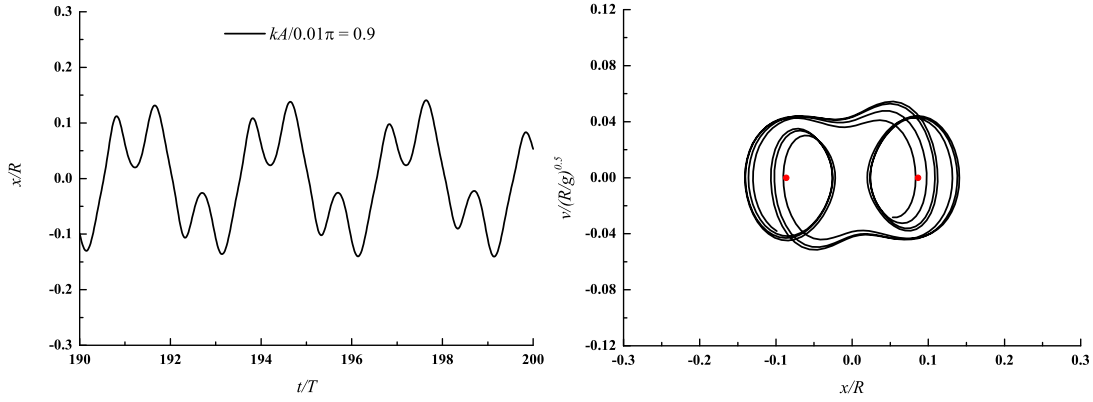

(c) $kA/0.01\pi = 0.9$

Figure 9: Time responses (left) and phase diagrams (right) of the internal nonlinear PTO to regular waves of frequency $kR = 0.4$

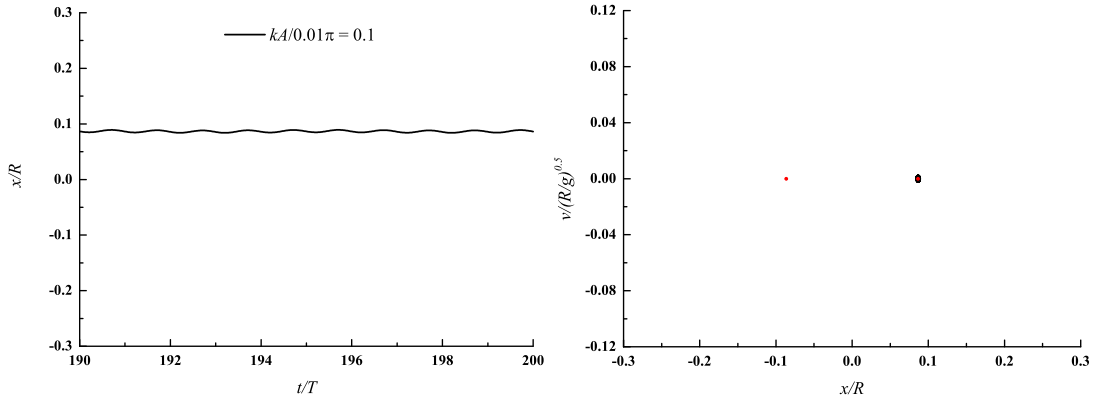

(a) $kA/0.01\pi = 0.1$

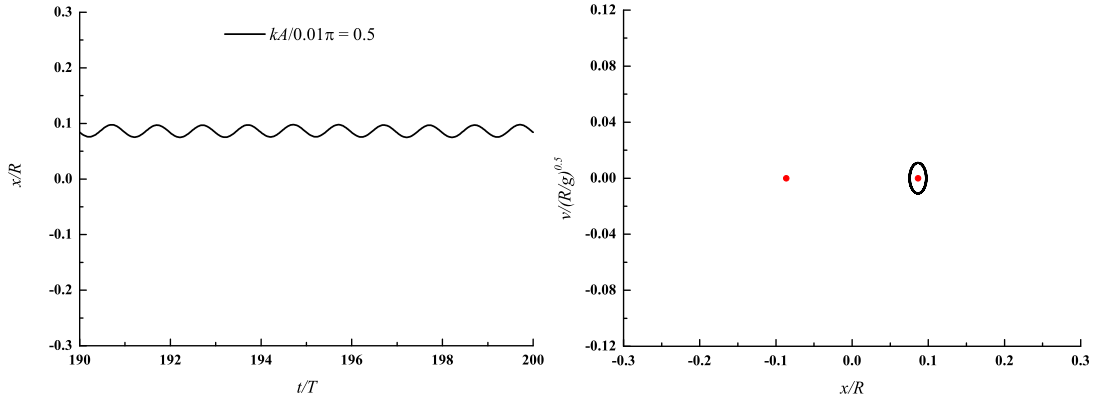

(b) $kA/0.01\pi = 0.5$

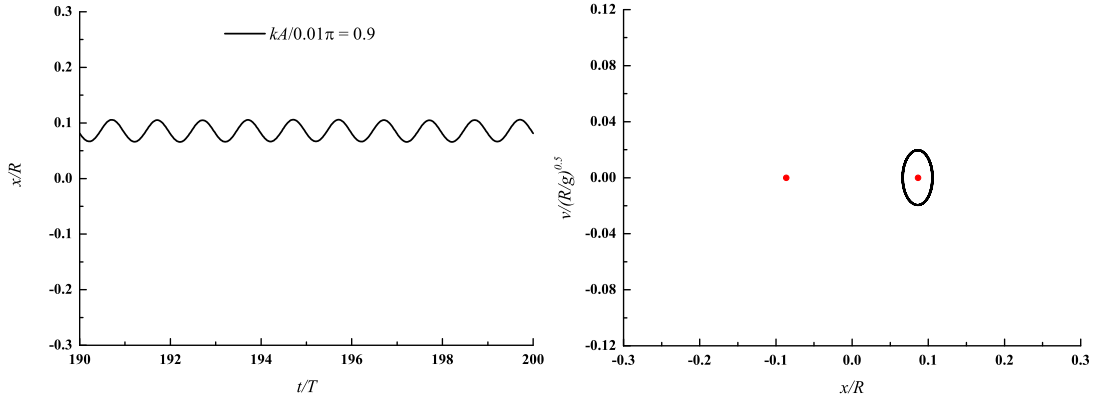

(c) $kA/0.01\pi = 0.9$

Figure 10: Time responses (left) and phase diagrams (right) of the internal nonlinear PTO to regular waves of frequency $kR = 1.0$

When the wave amplitude increases to a medium amplitude such as $kA/0.01\pi = 0.5$, the internal mass snaps aperiodically between the two stable equilibrium positions, as shown in Fig. 8(b). This aperiodic response is also called as intermittent snap-through. Further increase of the wave amplitude leads to the occurrence of the internal mass undergoing periodic snap-through. Figure 8(c) shows that with the wave amplitude $kA/0.01\pi = 0.9$, the internal mass produces large constant response loops enclosing both stable equilibrium positions. This result reveals that increasing the wave amplitude of regular waves will lead to three response regimes in order, i.e., local oscillation, aperiodic snap-through, and then periodic snap-through.

Apart from the low wave frequency $kR = 0.2$, results from high wave frequencies $kR = 0.4$ and 1.0 are also obtained, as shown in Figs. 9 and 10, respectively. Unlike the three response regimes observed at the wave frequency $kR = 0.2$, only two response regimes of the internal mass are shown for the wave frequency $kR = 0.4$ with the given range of wave amplitude. With the largest wave amplitude, i.e. $kA/0.01\pi = 0.9$, only the aperiodic snap-through takes place as shown by the phase diagram in Fig. 9(c). With smaller wave amplitudes such as $kA/0.01\pi = 0.5$ or 0.1, the local oscillation around one stable equilibrium position occurs, as revealed by Figs. 9(a) and 9(b). When the wave frequency becomes $kR = 1.0$, the increase of wave amplitude within the investigated range will not change the nature of response but only increase the amplitude of the response orbits. This is clearly illustrated in Fig. 10 where only local oscillation happens for all wave amplitudes. From Figs. $8 \sim 10$, it is concluded that the effect of wave amplitude on the dynamic response of the internal PTO is sensitive to the wave frequency.

From above, it is seen that the wave amplitude plays a significant role on the dynamic response of the internal nonlinear PTO. Consequently, the efficiency of the present WEC shall also be very dependent on the wave amplitude. The efficiency of the present WEC at various wave amplitudes is plotted in Fig. 11 in which the efficiencies with the linear PTO at the three wave frequencies are also shown in horizontal dash lines of different colors. Unlike the linear PTO, the

efficiency with the nonlinear snap-through PTO varies with the wave amplitude. At the small frequency $kR = 0.2$, the present snap-through WEC is able to extract more power than its linear counterpart over the wave amplitude range. For example, its efficiency is about 6 times of its linear counterpart with the wave amplitude $kA/0.01\pi = 0.77$. The great enhancement of power conversion efficiency is due to the periodic snap-through of the internal mass in the PTO as shown in Fig. 8(c). However, at higher frequencies such as $kR = 0.4$, the use of the nonlinear PTO is found to reduce the power extraction when the wave amplitude reaches a threshold. When the wave amplitude $kA/0.01\pi$ exceeds 0.66, it performs worse than the linear PTO. When the wave frequency further increases to $kR = 1.0$, the power extraction by using the nonlinear PTO is lower than that of the linear one over the present range of wave amplitude.

On the other hand, the response regimes are also reflected on the efficiency curve apart from the dynamic responses shown in Figs. 8, 9, and 10. At wave frequency $kR = 1.0$, the efficiency curve varies smoothly within the wave amplitude range from Fig. 11. This is because at this frequency only the local oscillation takes place without regime transition (see Fig. 10). While for the frequency $kR = 0.4$, a transition from local oscillation to aperiodic snap-through is noticed around the wave amplitude threshold $kA/0.01\pi = 0.66$. Therefore, there appears an abrupt change of power conversion efficiency near this threshold, as shown in Fig. 11. For the case of $kR = 0.2$, two transitions of response regimes are seen from Fig. 8. These two transitions occurs around $kA/0.01\pi = 0.33$ and 0.65 as seen from the efficiency curve.

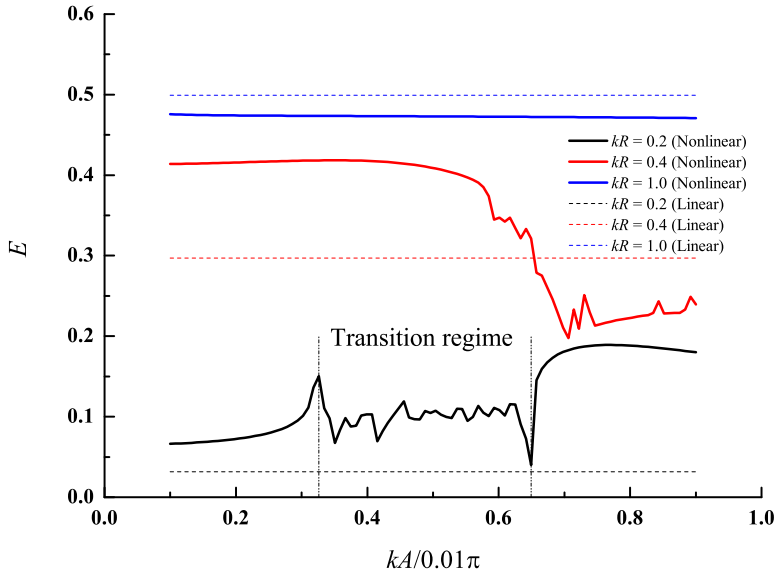

Figure 11: Efficiency of the nonlinear WEC varying with wave amplitude with regular wave of frequencies $kR = 0.2$, 0.4, and 1.0

4.2.2. Effect of wave frequency kR

In this section, the effect of wave frequency kR on the nonlinear WEC efficiency is studied. Again the other parameters on the right hand side of Eq. 14 are fixed the same as those in the convergence test except the wave parameters (kA and kR). The wave frequency kR ranges from 0.1 to 2 in this study. Similarly to Section 4.2.1, the time histories of the internal mass' relative surge displacement x and the phase diagram, $\dot{x}$ vs. x, are plotted at different kR, as shown in Figs. $8 \sim 10$. Table 1 summarizes the response regimes for regular waves with various wave amplitudes ($kA/0.01\pi = 0.1, 0.5, 0.9$) and frequencies ($kR = 0.2, 0.4, 1.0$). At small wave amplitude such as $kA/0.01\pi = 0.1$, only local oscillation response regimes are observed for all these frequencies $kR = 0.2$, 0.4 and 1.0 (see Figs. 8(a), 9(a), and 10(a)). When the wave amplitude increases to $kA/0.01\pi = 0.5$, the wave frequency shows its influence on the response regime. Both local oscillation and aperiodic response regimes are seen from Figs. 8(b), 9(b), and 10(b). Further increase of the wave amplitude to $kA/0.01\pi = 0.9$,

Table 1: Response regimes for regular waves with various wave amplitudes and frequencies

kR \ $kA/0.01\pi$	0.1	0.5	0.9
0.2	Local Oscillation	Aperiodic Snap-through	Periodic Snap-through
0.4	Local Oscillation	Local Oscillation	Aperiodic Snap-through
1.0	Local Oscillation	Local Oscillation	Local Oscillation

three response regimes are observed from Figs. 8(c), 9(c), and 10(c). At the low frequency $kR = 0.2$, the snap-through takes place as shown in Fig. 8(c). From Table 1, it can be concluded that the snap-through is prone to occur in large-amplitude and low-frequency waves.

The efficiency between the present snap-through WEC and the corresponding linear WEC is compared at various wave frequencies, as shown in Fig. 12. It is seen that the present snap-through WEC is able to extract more power than its linear counterpart at lower frequencies. However, the efficiency becomes smaller when the wave frequency is higher than a critical frequency. For the small wave amplitude $kA/0.01\pi = 0.1$, the critical frequency is $kR = 0.55$. Moreover, the efficiency curve with this small amplitude is smooth around the whole frequency range. This is simply because only the local oscillation response regime exists for the whole range. While for the other two wave amplitudes ($kA/0.01\pi = 0.5$ and 0.9), there appear transitions between different response regimes when varying wave frequencies.

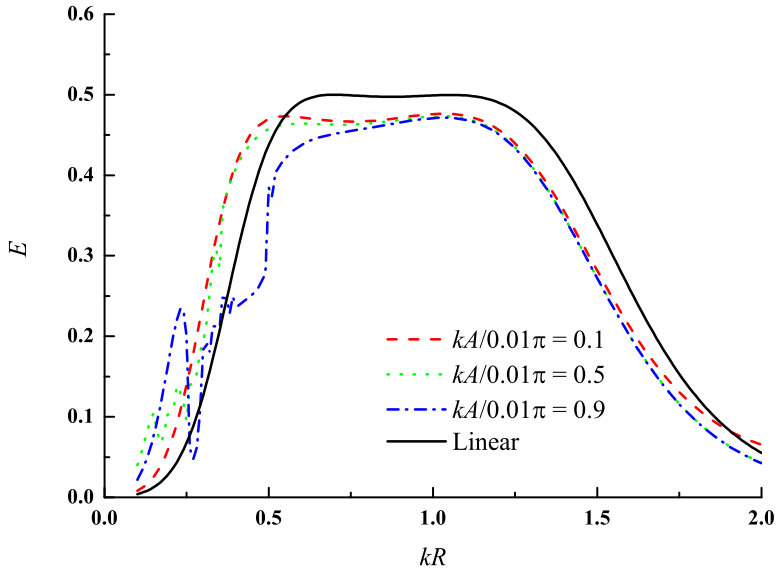

Figure 12: Efficiency of the nonlinear WEC varying with wave frequency with regular wave of amplitudes $kA/0.01\pi = 0.1$, 0.5, and 0.9

4.3. The nonlinear WEC in irregular waves

In this section, the effects of wave parameters of irregular waves including H_s and T_p on the efficiency of the nonlinear snap-through WEC are investigated. Before the studies on the effects of wave parameters, effects of the nonlinear snap-through PTO parameters l_0 and γ on the performance of the WEC are investigated. Here the significant wave height and peak wave period of the irregular wave are fixed at $H_s = 0.8$ and $T_p = 14$, respectively. The variations of efficiencies with the different nonlinear PTO parameters l_0 and γ are shown in Fig. 13 with the tuned frequency $k_0R = 0.4$. The maximum achievable efficiency with the nonlinear PTO is $E_{max} = 21\%$ which is about 38% higher than that with the linear PTO. In this case, the nonlinear snap-through mechanism operates with $l_0 = 0.2$ and $\gamma = 0.3$. Therefore, in the following parametric studies we fix the system parameters of the present WEC as: $s_0 = 0.1861$, $c = 0.0684$, $\gamma = 0.2$, $l_0 = 0.3$.

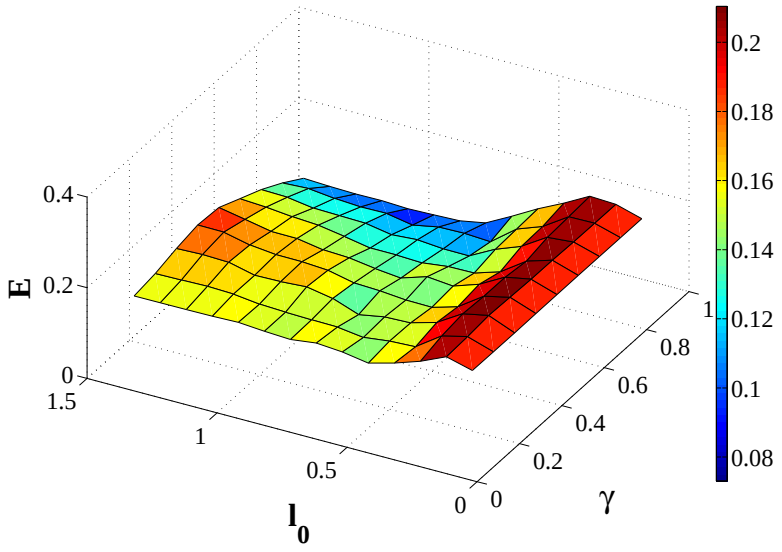

Figure 13: Effects of the nonlinear PTO parameters l_0 and γ on the power extraction efficiency of the WEC in irregular waves of $H_s = 0.8$ and $T_p = 14$ with the tuned frequency $k_0 R = 0.4$

4.3.1. Effect of significant wave height H_s

In this section, the effect of significant wave height H_s on the WEC efficiency is studied. The dimensionless significant wave height of the irregular wave is selected to range from $H_s = 0.2$ to 1.4. Three different dimensionless peak wave periods, i.e. $T_p = 5.6$, 14, and 22.4 are considered. Simulations of the WEC equipped with the linear PTO are also carried out for comparison. The efficiency of the WEC in waves of various wave significant wave heights H_s is plotted in Fig. 14. For the linear PTO, very slight efficiency variations are observed. This is not surprising since for the linear WEC system, i.e., the WEC with the linear PTO, its efficiency is independent on the incident wave amplitude. However, as for the nonlinear PTO, the change of the efficiency with various significant wave heights is significant. For example, along the $T_p = 5.6$ curve the efficiency of the WEC with $H_s = 0.2$ is about 54% larger than that with $H_s = 1.4$. For both $T_p = 14$ and 22.4 cases, an efficiency peak appears within the selected range of significant wave height, i.e., 21% and 6.4%, respectively. For the case of $T_p = 5.6$, the efficiency of the WEC with the nonlinear PTO monotonically

decreases with the significant wave height. On the other hand, the efficiency of the WEC with the nonlinear PTO is found larger than that with the linear PTO for both $T_p = 14$ and 22.4 cases. The maximum efficiency enhancement by use of the snap-through PTO is about 37.3% and 157% respectively. However, for the case of $T_p = 5.6$, the linear PTO has greater efficiency than the nonlinear counterpart. The maximum difference is about 6.6%. Therefore, the use of the snap-through mechanism is more preferable with higher peak wave period.

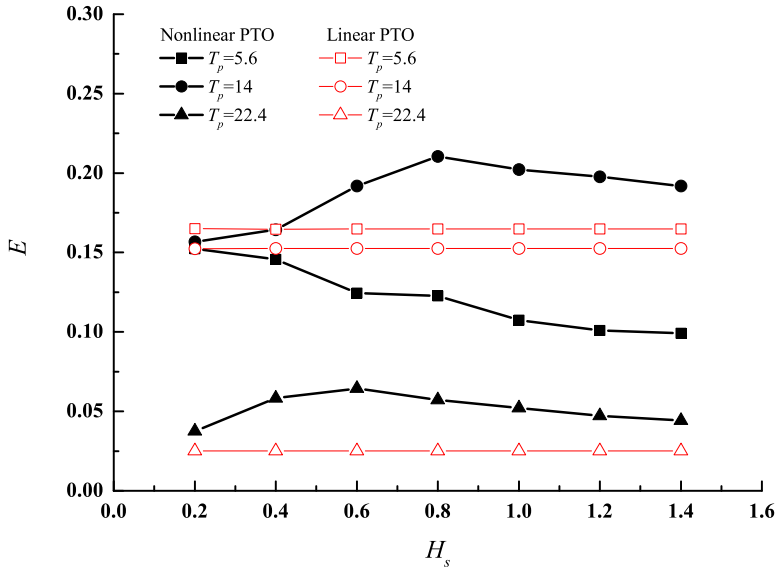

Figure 14: Effect of the significant wave height on the efficiency of the WEC

4.3.2. Effect of peak wave period T_p

In this section, the effect of peak wave period T_p on the WEC efficiency is studied. The dimensionless peak wave period of the irregular wave is selected to range from $T_p = 5.6$ to 22.4. Three different dimensionless significant wave heights, i.e. $H_s = 0.2$, 0.8, and 1.4 are considered. Results of the efficiency varying with peak wave period T_p are shown in Fig. 15. It is seen that the efficiency of WEC with the linear PTO is sensitive to the peak wave period rather than the significant wave height. This is also illustrated from Fig. 14. For the efficiency curve of the WEC containing the linear PTO, there appears

a peak at $T_p = 8.4$. For the case of the nonlinear PTO, both the significant wave height and the peak wave period influence the efficiency of the WEC. Moreover, the efficiency curves show a peak within the studied T_p range. For both the medium and large significant wave heights ($H_s = 0.8$ and 1.4), the peak efficiency appears at $T_p = 11.2$, while for the small significant wave height ($H_s = 0.2$), the peak efficiency is located at $T_p = 8.4$. The use of the nonlinear WEC leads to the peak shift of the efficiency curve.

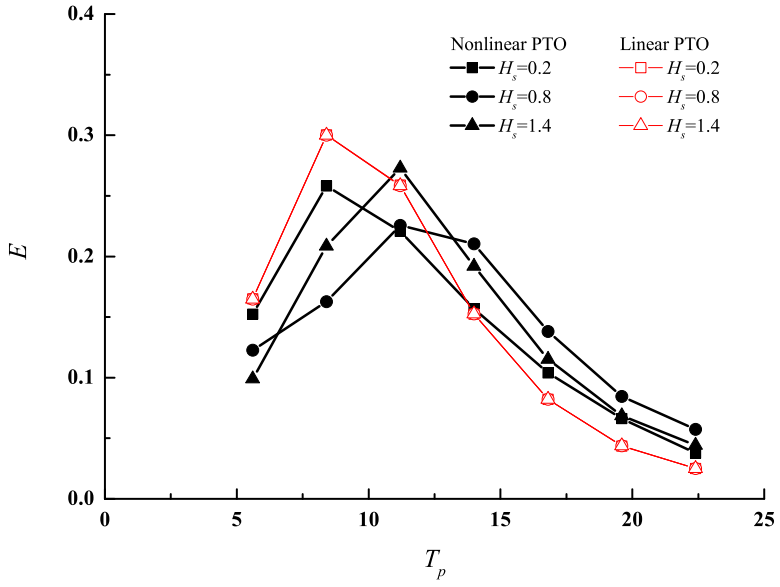

Figure 15: Effect of the peak wave period on the efficiency of the WEC

At last, to show the efficiency variation against both H_s and T_p, Table 2 lists the ratio of efficiencies between WECs with the nonlinear and linear PTOs ($E_{nonlinear}/E_{linear}$) in irregular waves. The significant wave height affects efficiency in the case of the nonlinear PTO, while it does not affect efficiency in the case of the linear PTO (see Fig. 14). Moreover, for the nonlinear PTO, the efficiency of the WEC is more sensitive to the peak wave period compared with the significant wave height.

Table 2: Ratio of efficiencies between WECs with the nonlinear and linear PTOs ($E_{nonlinear}/E_{linear}$) in irregular waves of various significant wave heights and peak wave periods

H_s \ T_p	5.6	8.4	11.2	14	16.8	19.6	22.4
0.2	0.92	0.86	0.85	1.03	1.27	1.52	1.50
0.4	0.88	0.69	0.67	1.08	1.55	1.91	2.33
0.6	0.75	0.56	0.81	1.26	1.73	2.13	2.57
0.8	0.74	0.54	0.87	1.38	1.68	1.93	2.29
1.0	0.65	0.58	0.97	1.33	1.51	1.78	2.08
1.2	0.61	0.64	1.02	1.30	1.47	1.68	1.89
1.4	0.60	0.70	1.06	1.26	1.40	1.57	1.77

5. Conclusions

In this paper, a submerged wave energy converter equipped with a nonlinear bistable snap-through PTO system is investigated. The equations of motion of this two DOF system are derived by the Euler-Lagrange equations. To solve these motion equations, a time-domain numerical method using the fourth-order predictor-corrector Adams-Bashforth-Moulton method is adopted. Both regular and irregular waves conditions are considered and compared with the results from a linear PTO. Moreover, parametric studies have been carried out to determine the optimum operating conditions of the bistable device in order to maximize the energy extraction efficiency. Through this study, the major conclusions are listed as follows:

(a) Snap-through of the internal mass in the PTO mechanism is prone to take place in large-amplitude and low-frequency incident waves;

(b) Three response regimes, i.e. local oscillation, aperiodic snap-through, and periodic snap-through, of the nonlinear PTO system are observed under various wave conditions;

(c) The present snap-through WEC is able to extract more power than its linear counterpart in either lower-frequency regular waves or higher peak period irregular waves;

(d) The significant wave height affects efficiency in the case of the nonlinear PTO, while it has no influence on efficiency with the linear PTO. Moreover, the efficiency of the WEC with the nonlinear PTO is more sensitive to the peak wave period compared with the significant wave height.

In this study, what we consider is a two-dimensional problem since the hydrodynamic coefficients in two dimensions are available by using the efficient analytical method, i.e. the multipole expansion method. In the future development, the performance of the three-dimensional WEC consisting of a finite length cylinder and operating in the open sea will be carried out. For this problem, instead of analytical methods, it is necessary to use commercial software such as WAMIT to determine the hydrodynamic coefficients for the three-dimensional counterpart. Moreover, as seen from Eqs. 14 and 19, the efficiency of the present WEC is determined by multiple variables. In this study, the optimum condition for a nonlinear PTO is determined by fixing all other parameters. This only leads to sub-optimum conditions. In the future, it is necessary to perform multi-variable optimization in order to maximize the power capture of the present WEC.

Acknowledgement

The authors thank the two anonymous reviewers for their constructive comments and suggestions, which have greatly improved the quality of this paper. This work was financially supported by the Fundamental Research Funds for the Central Universities (WUT: 2017IVA009) and the National Natural Science Foundation of China (Grant No. 51609188, 11702244). These supports are gratefully acknowledged by the authors.

References

[1] A. F. de O. Falcão, Wave energy utilization: A review of the technologies, Renewable and Sustainable Energy Reviews 14 (3) (2010) 899–918.

[2] I. López, J. Andreu, S. Ceballos, I. Martínez de Alegra, I. Kortabarria, Review of wave energy technologies and the necessary power-equipment, Renewable and Sustainable Energy Reviews 27 (2013) 413–434.

[3] J. Falnes, A review of wave-energy extraction, Marine Structures 20 (4) (2007) 185–201.

[4] X. Zhang, J. Yang, L. Xiao, Numerical study of an oscillating wave energy converter with nonlinear snap-through power-take-off systems in regular waves, in: the 24th International Ocean and Polar Engineering Conference, 2014, pp. 522–527.

[5] X. Zhang, J. Yang, Power capture performance of an oscillating-body wec with nonlinear snap through pto systems in irregular waves, Applied Ocean Research 52 (2015) 261–273.

[6] J. F. Gaspar, M. Kamarlouei, A. Sinha, H. Xu, M. Calvário, F.-X. Faÿ, E. Robles, C. G. Soares, Speed control of oil-hydraulic power take-off system for oscillating body type wave energy converters, Renewable Energy 97 (2016) 769–783.

[7] H. Shi, F. Cao, Z. Liu, N. Qu, Theoretical study on the power take-off estimation of heaving buoy wave energy converter, Renewable Energy 86 (2016) 441–448.

[8] D. V. Evans, A theory for wave-power absorption by oscillating bodies, Journal of Fluid Mechanics 77 (1) (1976) 1–25.

[9] D. V. Evans, D. C. Jeffrey, S. H. Salter, J. R. M. Taylor, Submerged cylinder wave energy device: theory and experiment, Applied Ocean Research 1 (1) (1979) 3–12.

[10] J. P. DAVIS, Wave energy absorption by the bristol cylinder - linear and non-linear effects, Proceedings of the Institution of Civil Engineers 89 (3) (1990) 317–340.

[11] D. V. Evans, R. Porter, Wave energy extraction by coupled resonant absorbers, Philosophical Transactions of the Royal Society A: Mathematical, Physical and Engineering Sciences 370 (1959) (2012) 315–344.

[12] S. Crowley, R. Porter, D. V. Evans, A submerged cylinder wave energy converter, Journal of Fluid Mechanics 716 (2013) 566–596.

[13] S. H. Crowley, R. Porter, D. V. Evans, A submerged cylinder wave energy converter with internal sloshing power take off, European Journal of Mechanics - B/Fluids 47 (2014) 108–123.

[14] M. Anbarsooz, M. Passandideh-Fard, M. Moghiman, Numerical simulation of a submerged cylindrical wave energy converter, Renewable Energy 64 (2014) 132–143.

[15] N. Y. Sergiienko, B. S. Cazzolato, B. Ding, P. Hardy, M. Arjomandi, Performance comparison of the floating and fully submerged quasi-point absorber wave energy converters, Renewable Energy 108 (2017) 425C437.

[16] L. Wang, J. Isberg, Nonlinear passive control of a wave energy converter subject to constraints in irregular waves, Energies 8 (7) (2015) 6528–6542.

[17] U. A. Korde, Phase control of floating bodies from an on-board reference, Applied Ocean Research 23 (5) (2001) 251–262.

[18] A. Babarit, G. Duclos, A. H. Clément, Comparison of latching control strategies for a heaving wave energy device in random sea, Applied Ocean Research 26 (5) (2004) 227–238.

[19] A. Babarit, A. H. Clément, Optimal latching control of a wave energy device in regular and irregular waves, Applied Ocean Research 28 (2) (2006) 77–91.

[20] A. Babarit, M. Guglielmi, A. H. Clément, Declutching control of a wave energy converter, Ocean Engineering 36 (12-13) (2009) 1015–1024.

[21] R. Genest, F. Bonnefoy, A. H. Clément, A. Babarit, Effect of non-ideal power take-off on the energy absorption of a reactively controlled one degree of freedom wave energy converter, Applied Ocean Research 48 (2014) 236 – 243.

[22] E. Ozkop, I. H. Altas, Control, power and electrical components in wave energy conversion systems: A review of the technologies, Renewable and Sustainable Energy Reviews 67 (2017) 106–115.

[23] X. Zhang, J. Yang, W. Zhao, L. Xiao, Effects of wave excitation force prediction deviations on the discrete control performance of an oscillating wave energy converter, Ships and Offshore Structures 11 (4) (2016) 351–368.

[24] X. Xiao, L. Xiao, T. Peng, Comparative study on power capture performance of oscillating-body wave energy converters with three novel power take-off systems, Renewable Energy 103 (2017) 94–105.

[25] C. Liang, L. Zuo, On the dynamics and design of a two-body wave energy converter, Renewable Energy 101 (2017) 265–274.

[26] R. Ramlan, M. J. Brennan, B. R. Mace, I. Kovacic, Potential benefits of a non-linear stiffness in an energy harvesting device, Nonlinear Dynamics 59 (4) (2010) 545–558.

[27] J. H. Mathews, D. F. Kurtis, Numerical Methods Using MATLAB 3rd edition, Prentice Hall, 1999.

[28] J. N. Newman, The exciting forces on fixed bodies in waves, Journal of Ship Research 6 (3) (1962) 10–17.

[29] W. Cummins, The impulse response function and ship motions, Navy Department, David Taylor Model Basin, 1962.

[30] P. C. Vicente, A. F. de O. Falcão, L. M. C. Gato, P. A. P. Justino, Dynamics of arrays of floating point-absorber wave energy converters with inter-body and bottom slack-mooring connections, Applied Ocean Research 31 (4) (2009) 267–281.

[31] D. V. Evans, R. Porter, Wave-free motions of isolated bodies and the existence of motion-trapped modes, Journal of Fluid Mechanics 584 (2007) 225–234.

[32] O. Faltinsen, Sea Loads on Ships and Offshore Structures, Cambridge University Press, 1990.

[33] M. Greenhow, S. I. Ahn, Added mass and damping of horizontal circular cylinder sections, Ocean Engineering 15 (5) (1988) 495–504.

[34] A. F. de O. Falcão, Modelling and control of oscillating-body wave energy converters with hydraulic power take-off and gas accumulator, Ocean Engineering 34 (14-15) (2007) 2021–2032.

[35] Y. Goda, Random Seas and Design of Maritime Structures 2nd Edition, World Scientific, Singapore, 2000.

[36] D. R. Johnson, M. Thota, F. Semperlotti, K. W. Wang, A bi-stable oscillator for increasing damping and providing passive adaptability, in: SPIE Smart Structures and Materials+ Nondestructive Evaluation and Health Monitoring, 2012, pp. 83410A–83410A.

Appendix A. Frequency-domain analysis of a linear PTO inside the submerged wave energy converter

In this analysis, a submerged WEC equipped with a linear PTO (shown in Fig. 1) consisting of a simple spring-mass-damper system will be investigated. The non-dimensional equations of motion for this WEC are

$$(m + M + A_{11})\, L^2\ddot{\theta} + mL\ddot{x} + B_{11}L^2\dot{\theta} + (1 - M - m)L\theta = F_{ex}L \tag{A.1}$$

$$mL\ddot{\theta} + m\ddot{x} + c\dot{x} + 2s_0 x = 0 \tag{A.2}$$

Defining the cylinder's surge velocity $L\dot{\theta} = Re(Ue^{-i\omega t})$ and the internal mass' relative horizontal velocity $\dot{x} = Re(ue^{-i\omega t})$, one obtains

$$(B_{11} - i\omega I)U = F_{ex} + im\omega u \tag{A.3}$$

$$-im\omega(u + U) + cu + 2ius_0/\omega = 0 \tag{A.4}$$

where $I = m + M + A_{11} - C_0/\omega^2$, $C_0 = (1 - M - m)/L$. Thus we have

$$Zu = im\omega F_{ex} \tag{A.5}$$

where $Re(Z) \equiv B_{11}c + m^2\omega^2 - I\omega^2\left(m - 2s_0/\omega^2\right)$, $Im(Z) \equiv -\omega\left[B_{11}\left(m - 2s_0/\omega^2\right) + cI\right]$, and $|F_{ex}| = A\sqrt{B_{11}/\pi\omega}$.

The extracted power is calculated by

$$P = \frac{1}{2}c|u|^2 \tag{A.6}$$

The total power carried by the incident wave is

$$P_w = \frac{A^2}{4\pi\omega} \tag{A.7}$$

Therefore the power extraction efficiency of the WEC is

$$E \equiv \frac{P}{P_w} = \frac{2cm^2\omega^2 B_{11}}{(B_{11}c + k_1)^2 + \omega^2(k_2 + cI)^2} \tag{A.8}$$

where $k_1 = m^2\omega^2 - I\omega^2\left(m - 2s_0/\omega^2\right)$ and $k_2 = B_{11}\left(m - 2s_0/\omega^2\right)$.

Equation A.8 reveals that both s_0 and c can be tuned to achieve high efficiency. Note both k_1 and k_2 are independent of c, and the following

$$\frac{(B_{11}c + k_1)^2}{c} = B_{11}^2 c + 2B_{11}k_1 + \frac{k_1^2}{c} \geq 4B_{11}k_1 \tag{A.9}$$

$$\frac{\omega^2(k_2 + cI)^2}{c} = \omega^2 \left(\frac{k_2^2}{c} + 2k_2 I + I^2 c \right) \geq 4\omega^2 I k_2 \tag{A.10}$$

then

$$E \leq \frac{2cm^2\omega^2 B_{11}}{4B_{11}k_1 + 4\omega^2 I k_2} \tag{A.11}$$

The maximum efficiency is achieved when

$$c^2 = \frac{k_1^2}{B_{11}^2} = \frac{k_2^2}{I^2} \tag{A.12}$$

With Eq. A.12, the optimal spring stiffness and damping can be determined at a given frequency ω_0,

$$2s_0 = m\omega_0^2 - \frac{I(\omega_0)m^2\omega_0^4}{B_{11}^2(\omega_0) + \omega_0^2 I^2(\omega_0)} \tag{A.13}$$

$$c = \frac{B_{11}(\omega_0)m^2\omega_0^2}{B_{11}^2(\omega_0) + \omega_0^2 I^2(\omega_0)} \tag{A.14}$$

And the maximum efficiency can be determined after some algebra

$$E_{max} = \frac{1}{2} \tag{A.15}$$

This result has also been found by other researchers [8, 12]. At this optimal condition, furthermore, the oscillation amplitudes for both the internal mass and the submerged cylinder can be determined as

$$\left|\frac{x}{A}\right|^2 = \frac{m^2 B_{11}/\omega\pi}{(B_{11}c + k_1)^2 + \omega^2(k_2 + cI)^2} \tag{A.16}$$

$$\left|\frac{L\theta}{A}\right|^2 = \left|\frac{x}{A}\right|^2 \left[\left(\frac{2s_0}{m\omega^2} - 1 \right)^2 + \frac{c^2}{m^2\omega^2} \right] \tag{A.17}$$